



Application of Geogrids in Stabilizing Rail Track Substructure

Syed Khaja Karimullah Hussaini* and Kumari Sweta

Railway Engineering, Department of Civil and Environmental Engineering, Indian Institute of Technology Patna, Patna, India

OPEN ACCESS

Edited by:

Eduardo Cabrita Fortunato,
National Laboratory for Civil
Engineering, Portugal

Reviewed by:

Ruilin You,
China Academy of Railway
Sciences, China
Sujit Kumar Dash,
Indian Institute of Technology
Kharagpur, India

*Correspondence:

Syed Khaja Karimullah Hussaini
hussaini@iitp.ac.in

Specialty section:

This article was submitted to
Transportation and Transit Systems,
a section of the journal
Frontiers in Built Environment

Received: 21 August 2019

Accepted: 11 February 2020

Published: 25 February 2020

Citation:

Hussaini SKK and Sweta K (2020)
Application of Geogrids in Stabilizing
Rail Track Substructure.
Front. Built Environ. 6:20.
doi: 10.3389/fbuil.2020.00020

Large-scale direct shear tests were conducted to assess the performance of geogrid-reinforced ballast-sub-ballast interface followed by triaxial tests to explore the deformation and degradation response of geogrid-reinforced ballast under cyclic loading. While the direct shear testing was performed at applied normal stresses (σ_n) ranging from 20 to 100 kPa and rate of shearing (S_r) from 2.5 to 10.0 mm/min, the cyclic triaxial tests were performed to capture the role of loading frequency (f) ranging from 10 to 40 Hz. Fresh granite ballast and sub-ballast with mean particle size (D_{50}) of 42 and 3.5 mm, and five geogrids having different aperture shapes and sizes (A) were used in this study. The tests results indicated that the behavior of ballast-sub-ballast interface is highly influenced by σ_n and S_r . The friction (φ) and dilation angles (ψ) of unreinforced and geogrid-reinforced ballast-sub-ballast interface is found to reduce from 67.96 to 47.82° and 14.56 to 3.34° with the increase in σ_n and S_r . Marsal's Breakage (B_g : an index to quantify the breakage of ballast) of unreinforced ballast was found to increase from 2.84 to 6.69% with the increase in σ_n and S_r . However, the inclusion of geogrids significantly enhanced the friction angle (φ), reduced the extent of dilation angle (ψ), and minimized B_g . The interface efficiency factor (α) and B_g were found to be a function of A/D_{50} ratio. Accordingly, a model is developed using multiple linear regression analysis to predict the values of φ , ψ , and B_g in terms of the input parameters σ_n , S_r , and A/D_{50} ratio. The results from triaxial tests indicate the deformation and degradation behavior of ballast under cyclic loading conditions to be influenced by the loading frequency (f). The extent of I_d and S_v of unreinforced ballast increases from 5.48 to 28.32 mm and 20.13 to 45.40 mm with the increase in f . The value of B_g increased from 4.3 to 11.69% when the value of f was increased from 10 to 40 Hz. Similarly, the extent of lateral and vertical deformation of ballast was found to be a function of A/D_{50} ratio.

Keywords: geosynthetics, ballast-sub-ballast interface, direct shear test, cyclic loading, friction angle (φ), settlement (S_v), loading frequency (f), process simulation test (PST) apparatus

INTRODUCTION

Railways are one of the most economical modes of transportation for moving freight as well as passengers from one place to another. With the rapid increase in population and the associated traffic congestion on highways, the demand for high-speed railway lines is on rise. However, the inherent effect of the introduction of high-speed trains is to induce additional cyclic stresses on the substructure of a railway track that comprises mainly of ballast and sub-ballast layers. Ballast distributes the applied train load to the sub-ballast layer at an acceptable level while maintaining the track alignment and allowing the quick drainage of water. On the other hand, the sub-ballast

reduces the extent of stress being transferred to the soil beneath and also acts as a filter medium thereby preventing the upward migration of subgrade soil into the ballast layer. However, due to continuous passage of trains, ballast being unbound in nature undergoes a significant amount of lateral deformation and particle degradation which directly contributes to track settlement. The excessive deformation and degradation of ballast leads to track misalignment that calls for either the imposition of speed restrictions or the conduction of costly track maintenance operations. In this view, the railway organizations around the world have recently started using the geogrids for stabilizing the railway tracks. In practice, the geogrids are generally placed at the bottom of ballast layer (i.e., at ballast-sub-ballast interface) so that the same will not obstruct the track maintenance process. Once in place, geogrids generates non-displacement boundary condition that limits the lateral movement of ballast that subsequently reduces vertical settlement and deformation of ballast.

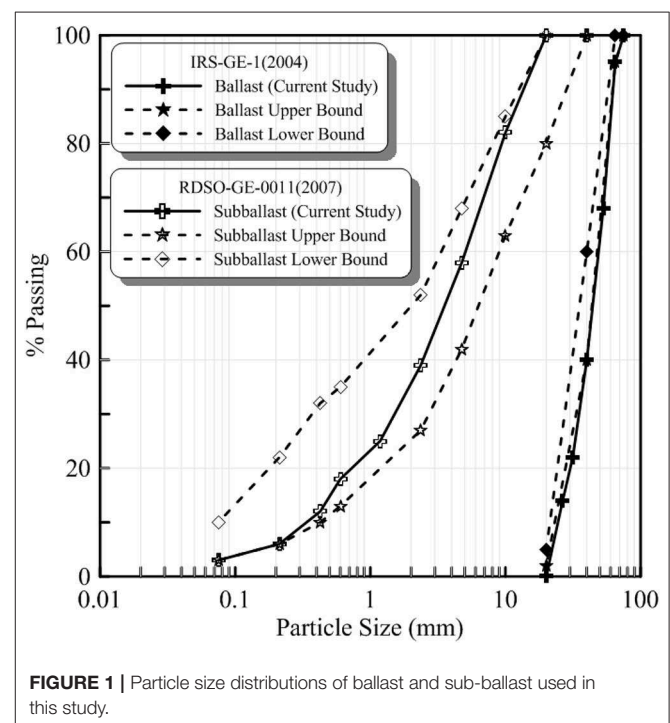
Realizing the importance of geogrids in rail track application, several researchers have studied the role of geogrids on coarse granular medium under direct shear conditions (Lee and Manjunath, 2000; Liu et al., 2009; Palmeira, 2009; Anubhav and Basudhar, 2010, 2013; Hussaini et al., 2012; Indraratna et al., 2012; Moraci et al., 2014; Sayeed et al., 2014; Biabani and Indraratna, 2015; Liu and Martinez, 2015; Vieira et al., 2015; Choudhary and Krishna, 2016; Liu F.-Y. et al., 2016; Liu S. et al., 2016; Afzali-Nejad et al., 2017; Guler and Khosrowshahi, 2017; Mvelase et al., 2017; Chen et al., 2018; Sweta and Hussaini, 2018, 2019a; Mirzaalimohammadi et al., 2019). Liu et al. (2009) have determined the shear behavior of granular soils stabilized with PET-yarn geogrids. On the other hand, Makkar et al. (2017) have evaluated the behavior of sand when reinforced with geogrid in three dimensional forms. Biabani and Indraratna (2015) have investigated the behavior of sub-ballast when stabilized with geogrids and geomembranes. Indraratna et al. (2012) and Hussaini et al. (2012) have explored the shear behavior of various ballast-geogrid interfaces at constant shearing rate of 2.5 mm/min. Sweta and Hussaini (2018, 2019a) have evaluated the shear behavior of ballast at different applied normal stresses and rates of shearing when stabilized with various geogrids. Similarly, several studies have highlighted the benefits of geogrids in stabilizing ballast under cyclic loading conditions (Bathurst and Raymond, 1987; Matharu, 1994; Brown et al., 2007; Indraratna et al., 2007, 2013, 2015; Mishra et al., 2014; Hussaini et al., 2015a,b, 2016; Biabani et al., 2016; Nimbalkar and Indraratna, 2016). Shin et al. (2002) highlighted the beneficial effect of reinforcement in reducing settlement when a layer of geogrid and geotextiles was placed at the interface of the subgrade and sub-ballast layer. Moreover, Nimbalkar and Indraratna (2016) have evaluated the benefits of inclusion of geosynthetics and rubber shock mats in the critical section of track through a field trial. Indraratna et al. (2015) and Biabani et al. (2016) have investigated the behavior of geocell-reinforced sub-ballast at different frequencies under cyclic loading conditions. Navaratnarajah and Indraratna (2017) have assessed the use of rubber mats in improving the deformation and degradation behavior ballast at different frequencies and axle load. Indraratna et al. (2013) and Hussaini et al. (2015b) are the only studies

that have captured the influence of geogrid aperture size (A) in stabilizing the railway ballast under cyclic loading conditions at a constant loading frequency (f) of 20 Hz. In addition, there are several studies that have shown the effect of loading frequency (f) on the behavior of unreinforced ballast under various cyclic loading conditions (Indraratna et al., 2010; Thakur et al., 2013; Sun et al., 2014, 2019). However, the role of geogrids in stabilizing railway ballast at different loading frequencies (f) has not been yet studied. Similarly, there are very limited studies that describe the influence of applied normal stress (σ_n) and rates of shearing (S_r) on various ballast-geogrid-sub-ballast interfaces under direct shear conditions. Moreover, a rail track under operating conditions may be subjected to different shearing rates depending upon the magnitude of cyclic stress and the train speed. In this context, a series of large-scale direct shear tests were carried out to study the influence of σ_n and S_r on ballast-geogrid-sub-ballast interface followed by large-scale cubical triaxial tests to determine the effect of loading frequency (f) on ballast with and without geogrids.

MATERIALS AND TESTING PROCEDURES

Materials

Fresh granite particles and a mixture of sand and crushed granite were used as ballast and sub-ballast, respectively. The particle size distributions (PSD) of ballast and sub-ballast used in the present study were as per the standards specified by Indian railways (IRSGE, 2004; RDSOGE, 2007; **Figure 1**). The particle size characteristics of ballast and sub-ballast are presented in **Table 1**. The maximum (D_{max}) and mean diameters (D_{50}) of sub-ballast were 20 and 3.5 mm and that of ballast were 65 and



42 mm, respectively. Five types of geogrids were used in the current study to stabilize the rail road ballast. These geogrids have different aperture shapes and sizes. The physical characteristics and technical specifications of geogrids (labeled *G1* to *G5*) used in the present study are described in **Table 2**.

Direct Shear Tests

A series of shear tests were performed using large-scale direct shear apparatus, having plan dimension of 450 × 450 mm and overall depth of 300 mm. The apparatus consists of two square boxes; the lower box is fixed in position while the upper box is allowed to move. The apparatus can allow application of normal stress and can capture the shear stresses up to 300 kN/m² and can allow shear displacements up to 100 mm. The dimensions of the apparatus and the capacity of load cells have been suitably selected to explicitly test coarse granular materials like railway ballast at high normal loading and strain rates. **Figure 2A** shows the schematic illustration of large-scale direct shear apparatus.

The specimen preparation involves the mixing of sieved ballast and sub-ballast separately in a required proportion conforming to the PSDs as specified in **Figure 1**. The lower box of shear apparatus was filled with a predetermined quantity of sub-ballast and then compacted in two layers with the help of a vibrating plate to attain a required density (γ_{sb}) of 2,000 kg/m³ which is the representative of typical field conditions. Then, the ballast is filled in the upper shear box and compacted in two layers with same vibrating plate to attain a field density (γ_b) of 1,470 kg/m³. In case of reinforced samples, a layer of geogrid is installed at the interface of two shear boxes and fixed with the clamping screws after the compaction of sub-ballast in lower shear box. To reduce the extent of particle breakage during vibration, a 7 mm thick rubber pad was placed beneath the vibrating plate. Tests were conducted at different applied normal stresses (σ_n) ranging from 20 to 100 kPa which is representative of typical track conditions under low confinement and shearing rates (S_r)

ranging from 2.5 to 10.0 mm/min. The tests were carried out up to the horizontal displacement of 67.5 mm that represents a horizontal strain of 15%.

Triaxial Tests Using Process Simulation Test (PST) Apparatus

A series of triaxial tests were carried out using large-scale process simulation test (PST) apparatus, consisting of a box of 950 mm length, 650 mm width, and 730 mm overall depth. The plan dimension of 950 mm represents the effective sleeper length that transfers the applied wheel load to the ballast beneath, as defined by Jeffs and Tew (1991) and Atalar et al. (2001). On the other hand, 650 mm represents the center-center spacing between the sleepers in the direction of rail. The mid portion of the two side walls parallel to rails (i.e., along the direction of passage of train) consists of five independent movable plates each measuring 650 mm in width and 75 mm in height. A small gap of 1 mm was provided to allow the free movement of plates in lateral direction. The maximum allowable lateral displacement of each plate is 100 mm that corresponds to a lateral strain (ϵ_3) of 10.52%. The apparatus used in the current study is similar to that used by Hussaini (2013) and Indraratna et al. (2013) but with five independently movable side walls on both the sides. The apparatus can be used to apply a vertical dynamic load of 200 kN at frequencies of up to 50 Hz. **Figure 2B** illustrates the schematic diagram of process simulation test apparatus.

The specimen preparation involved the placement of sub-ballast (150 mm thick), comprising of crushed granite-sand mixture, in two layers of 75 mm each and their compaction with the help of a vibrating plate to attain a required density (γ_{sb}) of 2,000 kg/m³. This was overlain by a ballast layer of 380 mm that was placed in three equal layers and compacted to achieve a target field density (γ_b) of 1,520 kg/m³. It is to be mentioned here that in both the series of tests the ballast particles were painted with bright yellow spray paint in order to clearly distinguish the broken pieces of ballast from underlying sub-ballast. A rail-sleeper assembly (wooden sleeper: 900 × 250 × 150 mm) was then placed over the compacted ballast and the spaces around the sleeper were filled with crib ballast. The rail section used was MR-52 section, as used by the Indian Railways on most of the broad gauge tracks. In case of reinforced samples, a layer of geogrid was placed at the ballast-sub-ballast interface as done in case of direct shear test samples.

TABLE 1 | Grain size characteristics of ballast and sub-ballast.

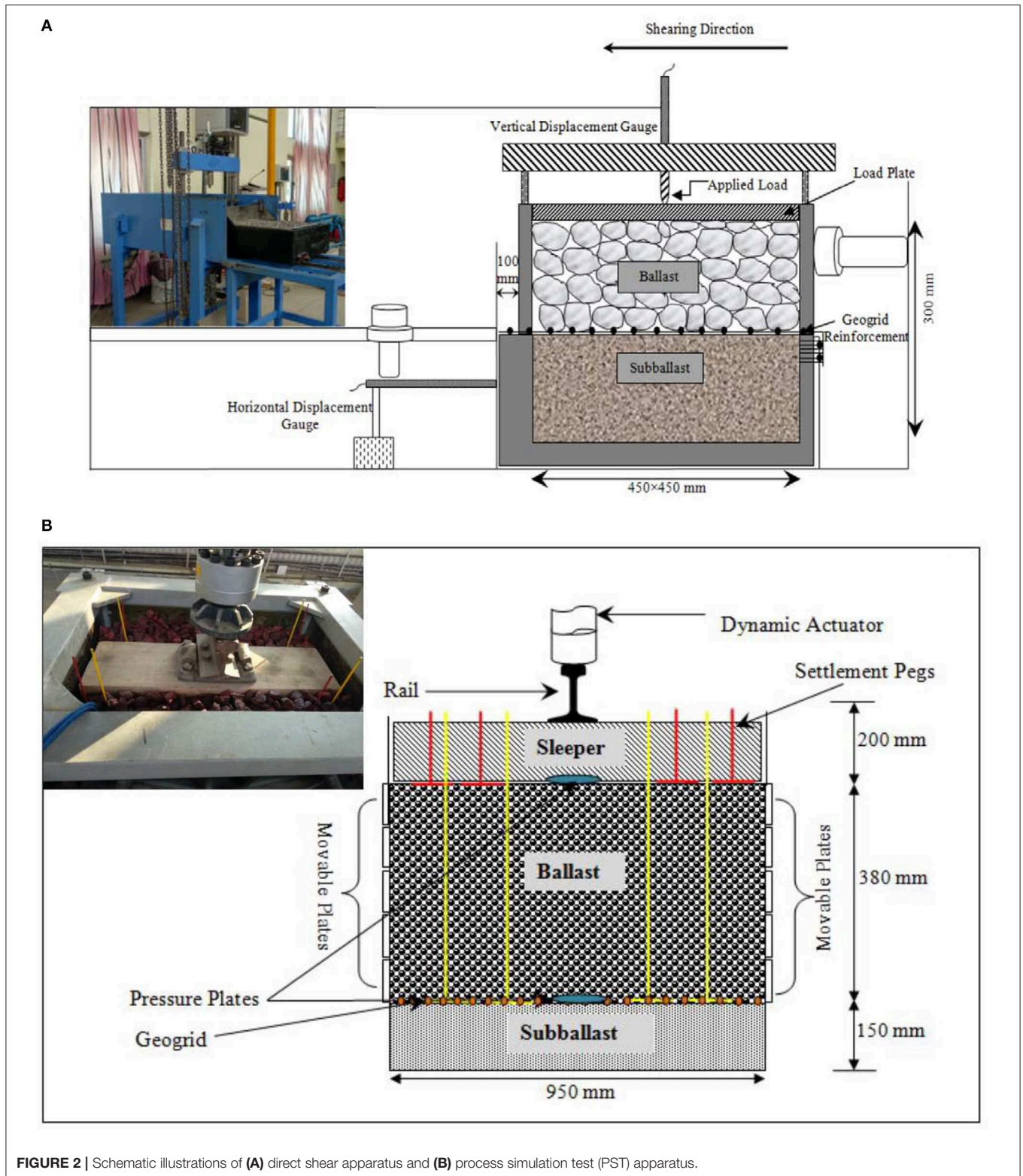
Material	D_{max} (mm)	D_{10} (mm)	D_{30} (mm)	D_{60} (mm)	D_{50} (mm)	C_u	C_c
Sub-ballast	20	0.35	1.7	5.0	3.5	14.29	1.65
Ballast	65	22	32	48	42	2.18	0.97

TABLE 2 | Physical characteristics and technical characteristics of geogrid used in the current study.

Characteristics	Properties	G1	G2	G3	G4	G5
Physical	Material	PP	PP	PP	PP	PP
	Aperture shape	Square	Triangular	Rectangular	Triangular	Square
	Aperture size (MD/CMD)	39/39	46/46	34/36	69/69	65/65
	Rib thickness	2.2/2.1	1.2/1.2	2.8/2.8	2.2/2.2	3.6/4.5
Technical	T_{ult}^a (kN/m)	30	19	40	21	30
	Tensile strength [®] 5% strain (kN/m)	21	14	28	15	22

^aUltimate Tensile Strength (manufacturer supplied values).

MD, machine direction; CMD, cross machine direction; PP, polypropylene.



A cyclic vertical stress of 300 kPa was applied onto the test specimen with the help of vertical dynamic actuator, and a confining pressure of 10 kPa was applied onto the two side walls

having five movable plates. It is well-known that the tendency of unbound ballast is to move laterally in outward direction (parallel to sleeper) under track operating conditions. Therefore,

the shorter walls were allowed to move laterally and the other two longitudinal walls were kept fixed to mimic the plane strain conditions ($\epsilon_2 = 0$) in the direction parallel to rails (i.e., along the direction of passage of train), as was also adapted earlier by Hussaini (2013) and Indraratna et al. (2013). Two earth pressure cells were placed at sleeper-ballast and ballast-sub-ballast interface to measure the vertical stresses during the test. The pressure cells used in the current study had the diameter of 230 mm and the thickness of 12 mm.

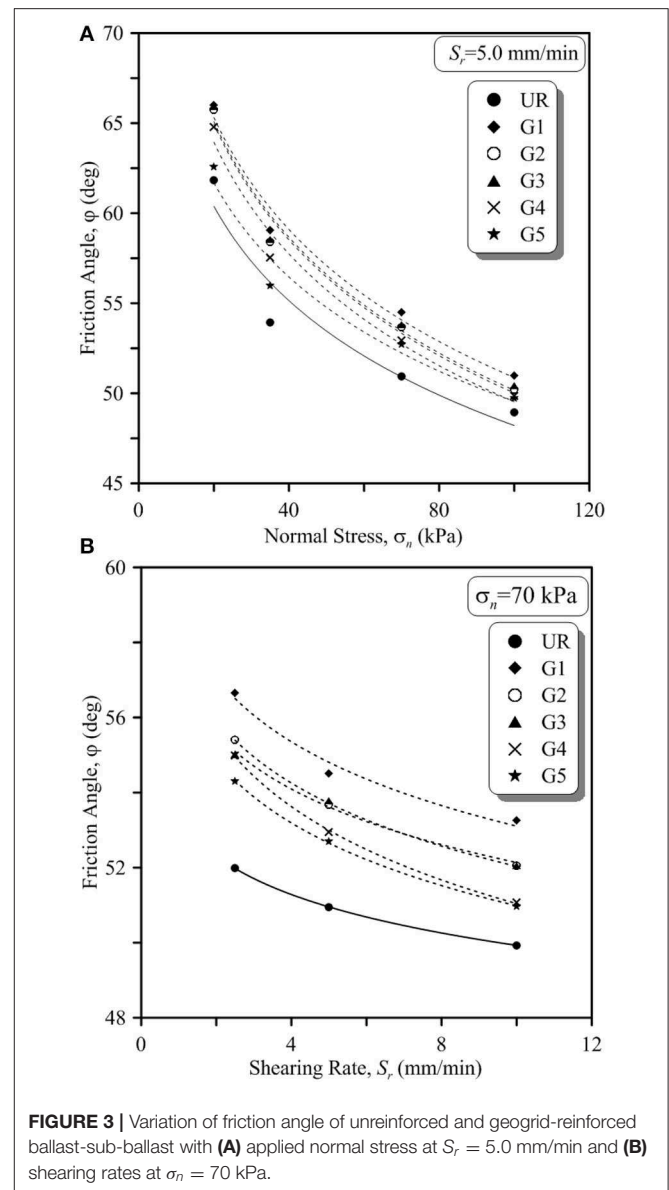
Tests were conducted at loading frequencies of 10, 20, 30, and 40 Hz which is representative of higher train speeds (~73–292 km/h, for an axle spacing of 2.02 m) and up to 250,000 load cycles (N). During the test, the lateral displacement of the movable plates and the vertical settlement of ballast were continuously recorded by the data acquisition system. The extent of vertical settlement was also recorded by placing four settlement plates at sleeper-ballast and ballast-sub-ballast interface. The test was halted at specific number of cycles to record the vertical settlement of ballast and sub-ballast layers. The ballast specimen was retrieved carefully and sieved after each test to evaluate the change in gradation and to quantify the breakage of particles owing to cyclic loading. **Figure 2B** shows the final arrangement of the test specimen ready for testing.

RESULTS AND DISCUSSION

Friction Angle (ϕ) of Ballast-Sub-Ballast Interface

Figure 3A shows the variation of friction angle (ϕ) with applied normal stress (σ_n) for unreinforced ballast-sub-ballast interface and that reinforced with various geogrids at $S_r = 5.0$ mm/min. It is seen that the ϕ of unreinforced ballast-sub-ballast interface reduces from 61.82 to 48.95° as σ_n increases from 20 to 100 kPa. The decrease in ϕ with the increase in σ_n is primarily due to the suppression of dilation and also because of the enhanced breakage of particles (as will be described in the latter sections of the paper) at higher normal stresses. Similar to the behavior of unreinforced interface, the apparent friction angle (δ) of ballast-sub-ballast interface when reinforced with geogrids $G1$ and $G2$ decreases from 66.02 to 50.97° and 65.76 to 50.22°, respectively, as σ_n increases from 20 to 100 kPa. A similar reduction in δ with the increase in σ_n is observed for other rates of shearing (S_r) but is not shown here for the sake of brevity. It is further observed that δ of all reinforced ballast-sub-ballast interfaces is greater than that of unreinforced interfaces (**Figure 3A**). For example, the insertion of geogrids $G4$ and $G5$ at ballast-sub-ballast interface increases the values of ϕ from 61.82 to 64.79° and 62.56°, respectively.

Figure 3B depicts the variation of friction angle (ϕ) with shearing rate (S_r) of unreinforced ballast-sub-ballast interface and that reinforced with various geogrids at $\sigma_n = 70$ kPa. The value of ϕ of unreinforced ballast-sub-ballast interface decreases from 51.98 to 49.93° as S_r is increased from 2.5 to 10.0 mm/min. The increasing rates of shearing have a similar effect on the friction angle of ballast-geogrid-sub-ballast interfaces. For example, the apparent friction angle (δ) of ballast-sub-ballast



reinforced with geogrid $G4$ and $G5$ reduced from 54.98 to 51.53° and 54.3 to 51° as S_r increased from 2.5 to 10.0 mm/min. The observation with respect to the variation of ϕ with S_r is in accordance with the studies conducted for ballast (Sweta and Hussaini, 2018) and sub-ballast (Biabani and Indraratna, 2015). In a practical sense, the reduced values of friction angles with the increase in shearing rates indicate the reduction in ballast performance with the increase in train speeds. However, it is seen that the geogrids enhance the friction angle of ballast-sub-ballast interface for all the applied shearing rates (**Figure 3B**), thereby highlighting their effectiveness in enhancing the ballast performance at higher train speeds. For instance, ϕ of unreinforced ballast-sub-ballast interface increased from 51.98 to 56.66° and 55.41° when stabilized with geogrid $G1$ and $G2$, respectively.

Dilation Angle (ψ) of Ballast-Sub-Ballast Interface

The dilation angle (ψ) of ballast-sub-ballast is mainly associated with the rate of dilation and is computed as the ratio of change in vertical displacement (d_v) to the change in horizontal displacement (d_h) (Equation 1; Bolton, 1986; Simoni and Houlby, 2006) and can be expressed as

$$\psi = \frac{d(d_v)}{d(d_h)} \tag{1}$$

Where ψ is the dilation angle, $d(d_v)$ is the change in vertical displacement, $d(d_h)$ is the change in horizontal displacement.

Figure 4 shows the variation of peak dilation angle (ψ) with peak friction angle (ϕ) of unreinforced ballast-sub-ballast interface and that stabilized with geogrids for different values of S_r . As expected, dilation angle (ψ) of both unreinforced and reinforced ballast-sub-ballast interface decreases with increasing values of σ_n . For example, the value of ψ in case of unreinforced ballast-sub-ballast interface and that reinforced with *G1* is found to decrease from 14.56 to 8.51° and 11.03 to 4.13° as σ_n increases from 20 to 100 kPa ($S_r = 2.5$ mm/min). Likewise, for $S_r = 5.0$ and 10.0 mm/min, the value of ψ decreases from 12.89 to 7.74° & 10.38 to 3.89° and 11.89 to 5.23° & 9.16 to 4.78°, respectively. It is further revealed that dilation angle (ψ) of both unreinforced and reinforced interface decreases with the increase in S_r . The value of ψ of unreinforced ballast-sub-ballast and that reinforced with *G1* decreases from 14.56 to 11.89° and 10.38 to 9.16° as S_r increases from 2.5 to 10.0 mm/min ($\sigma_n = 20$ kPa). Likewise, for other normal stresses of 35, 70, and 100 kPa, ψ decreases from 12.78 to 8.95° & 9.24 to 8.00°, 9.73 to 7.42° & 6.78 to 6.34°, and 8.51 to 5.23° & 4.13 to 3.35°, respectively. **Figure 5** also establishes the role of geogrids in diminishing the extent of dilation. For instance, reinforcement of ballast-sub-ballast interface with geogrid *G1* reduces the dilation angle (ψ) from 14.56 to 11.03° ($\sigma_n = 20$ kPa; $S_r = 2.5$ mm/min).

Breakage of Ballast (B_g) Under Shearing Conditions

The influence of applied normal stress (σ_n) and shearing rate (S_r) on the breakage of ballast for both unreinforced and reinforced ballast-sub-ballast interface is shown in **Figure 5**. It is revealed that B_g increases with the increase in σ_n and S_r . For example, B_g of unreinforced ballast increased from 3.33 to 5.26% as σ_n increased from 20 to 100 kPa. Furthermore, the value of B_g of unreinforced ballast increased from 3.41 to 5.72% as S_r enhanced from 2.5 to 10.0 mm/min ($\sigma_n = 35$ kPa; **Figure 5A**). A similar increase in B_g is observed for geogrid-reinforced ballast-sub-ballast interface. For instance, the ballast-sub-ballast interface when reinforced with geogrid *G1* and *G2*, the value of B_g increases from 2.49 to 3.49% and 2.56 to 3.56% as σ_n increases from 20 to 100 kPa. Furthermore, for the applied normal stress of 35 kPa, the value of B_g of ballast-sub-ballast interface reinforced with geogrid *G1* increases from 2.43 to 3.84% as S_r increases from 2.5 to 10.0 mm/min. It is evident from **Figure 5B** that insertion of geogrids at ballast-sub-ballast interface diminishes the extent of B_g in ballast. For example, in case of ballast reinforced with

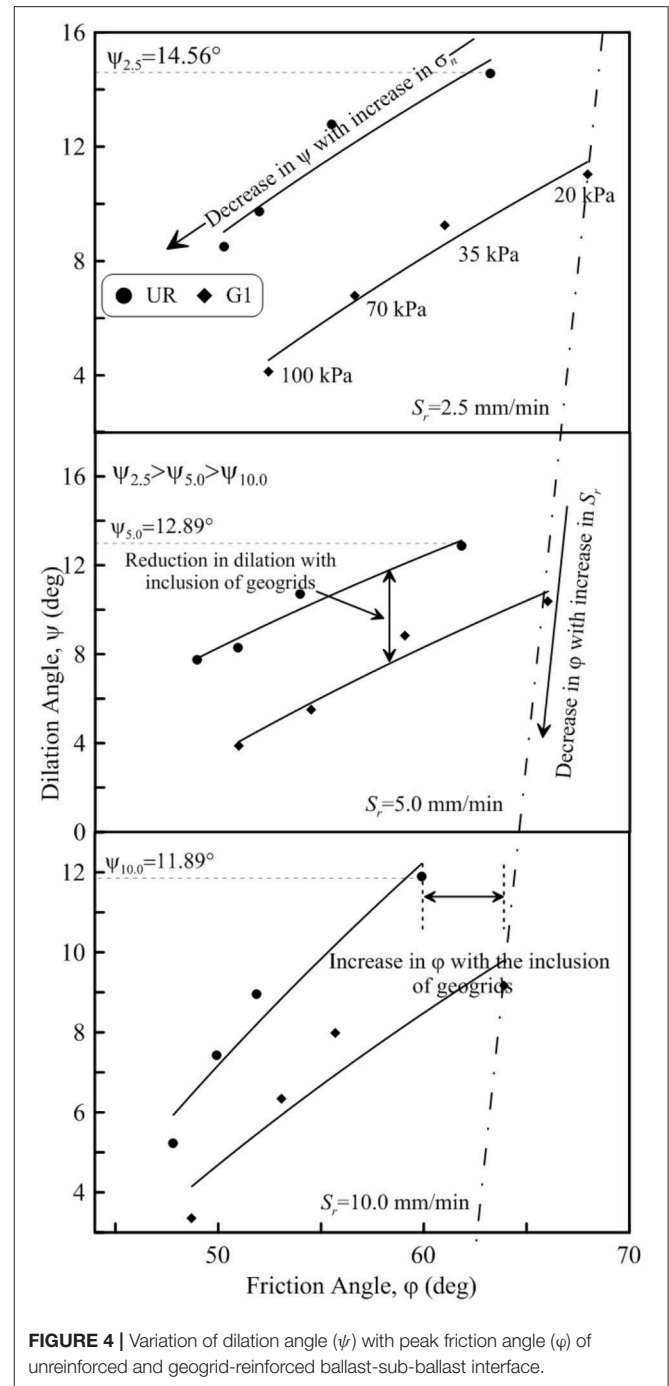
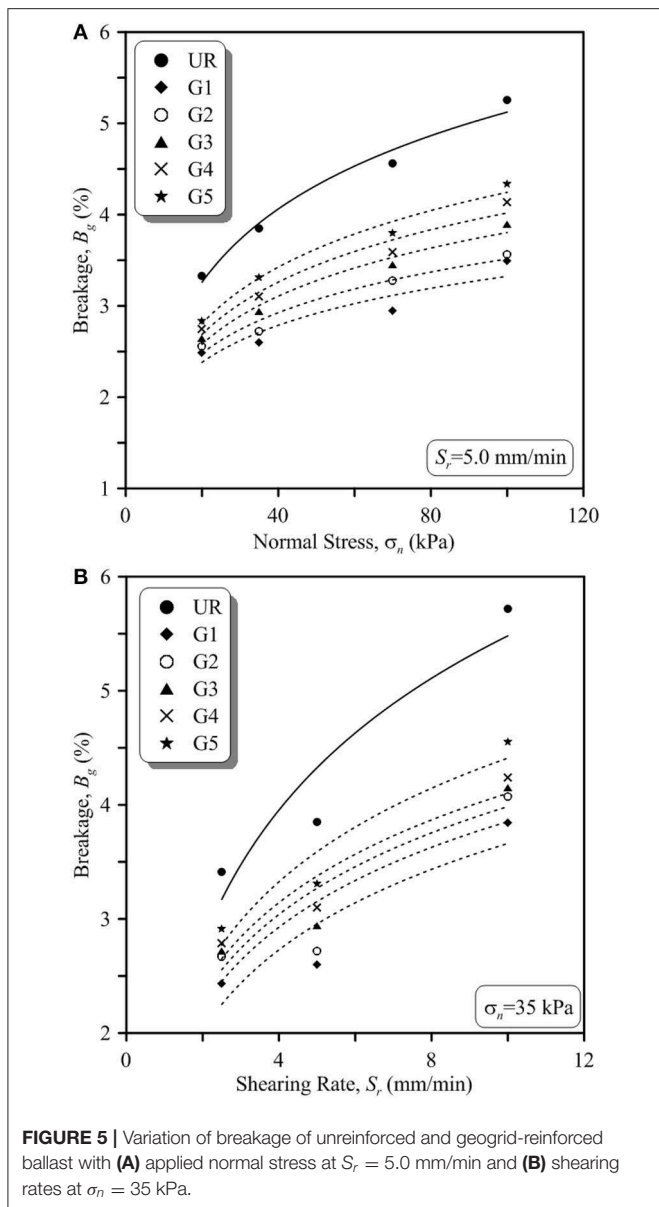


FIGURE 4 | Variation of dilation angle (ψ) with peak friction angle (ϕ) of unreinforced and geogrid-reinforced ballast-sub-ballast interface.

geogrid *G4* and *G5*, the value of B_g reduced from 3.85 to 3.10% and 3.31%, respectively ($\sigma_n = 35$ kPa; $S_r = 5.0$ mm/min).

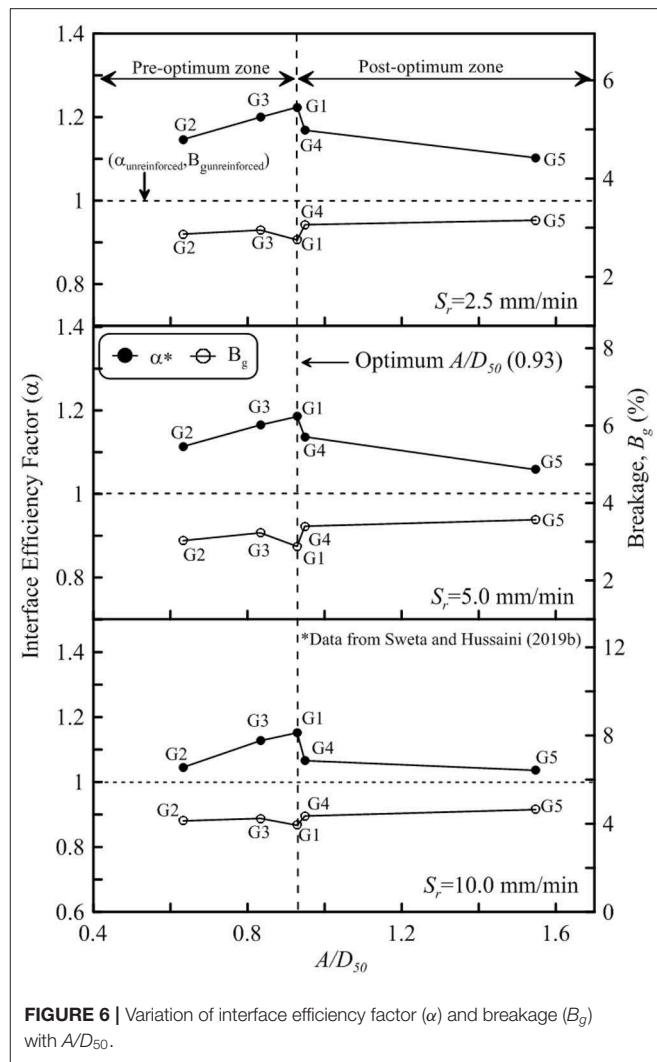
Regression Models to Determine of Friction (ϕ), Dilation Angles (ψ), and Breakage (B_g) of Ballast

To emphasize the role of geogrid aperture size (A) in enhancing the shear strength of ballast, the variation of interface efficiency factor (α) and ballast breakage (B_g) with A/D_{50} ratio for different



rates of shearing (S_r) are shown in **Figure 6**. It is revealed from **Figure 6** that as the value of α increases, the extent of B_g decreases. For instance, α attains the maximum value of 1.22 and B_g attains the minimum value of 2.75% at $A/D_{50} = 0.93$ (G1) and then α decreases to 1.10 and B_g increases to 3.15% at $A/D_{50} = 1.54$ (G5) (S_r : 2.5 mm/min). Similarly, for $S_r = 5.0$ and 10.0 mm/min, geogrid G1 with an A/D_{50} of 0.93 exhibits the maximum value of α of 1.19 and 1.15 which in turn exhibits the minimum breakage of 2.88 and 3.93%, respectively. This signifies that by suitably selecting the geogrids, the value of α could be enhanced significantly and breakage of ballast particles could be minimized.

It is well-known that the behavior of ballast under track operating conditions is governed by axle load, confining pressure and the train speed. In a real rail track environment, axle load is



transferred through the wheels of the trains while the confining pressure is generated due to particle-particle interaction, sleeper resistance, compaction stresses and overburden pressure. Moreover, a track under operating conditions will be often subjected to varying train speeds. Therefore, the field conditions are replicated in the laboratory, by suitably considering the values of applied normal stress and the rate of shearing (Sweta and Hussaini, 2019a). Moreover, the performance of a reinforced railway track depends upon the ratio of aperture size (A) of geogrids and the mean particle sizes, A/D_{50} ratio (Indraratna et al., 2012; Sweta and Hussaini, 2018, 2019a,b). In this context, regression models are developed to determine the values of friction angle (ϕ), dilation angle (ψ) and breakage of ballast (B_g) in terms of the input parameters σ_n , S_r , and A/D_{50} (Equations 2–7). Based on the variation of α , the A/D_{50} is classified into two zones (i.e., pre-optimum and post-optimum zone) as shown in **Figure 6**. The pre-optimum zone lies in the range of $0.63 \leq A/D_{50} \leq 0.93$ while the post-optimum zone lies in the range of $0.93 \leq A/D_{50} \leq 1.54$. The R^2 values for the models presented here vary from 0.88 to 0.90.

For $0.63 \leq A/D_{50} \leq 0.93$:

$$\varphi = -0.17\sigma_n - 0.55S_r + 4.41A/D_{50} + 66.19 \quad (2)$$

$$\psi = -0.07\sigma_n - 0.19S_r - 0.82A/D_{50} + 13.33 \quad (3)$$

$$B_g = 0.01\sigma_n + 0.17S_r - 0.36A/D_{50} + 1.96 \quad (4)$$

For $0.93 \leq A/D_{50} \leq 1.54$

$$\varphi = -0.15\sigma_n - 0.52S_r - 0.26A/D_{50} + 68.36 \quad (5)$$

$$\psi = 0.06\sigma_n - 0.26S_r + 0.19A/D_{50} + 13.10 \quad (6)$$

$$B_g = 0.01\sigma_n + 0.18S_r + 0.67A/D_{50} + 0.97 \quad (7)$$

Where φ = friction angle, ψ = dilation angle, B_g = breakage, σ_n = applied normal stress, S_r = rate of shearing.

The models presented here will help the rail practitioners to predict the values of φ , ψ , and B_g for ballast under both unreinforced and reinforced conditions once the values of input parameters (σ_n , S_r , and A/D_{50}) are known.

Lateral Displacement (l_d) and Vertical Settlement (S_v) of Ballast During Cyclic Loading

The evolution of lateral displacement (l_d) and vertical settlement (S_v) with number of load cycles (N) in case of unreinforced and geogrid-reinforced ballast at $f = 30$ Hz is shown in **Figure 7**. It is observed that the extent of l_d and S_v increases rapidly during the initial load applications (i.e., for values of N up to 50,000 cycles), and thereafter the displacements remain mostly the same. However, the extent of l_d and S_v of ballast reduces with the inclusion of geogrids. For example, insertion of geogrids $G1$ and $G3$ reduces the amount of l_d and S_v by 41 & 30% and 33 & 24%, respectively, in comparison to unreinforced ballast. On the other hand, the geogrid $G5$ reduces the values of l_d and S_v by 8% only. This is because the aperture sizes of geogrids $G1$ and $G3$ are nearer to the average particle size of ballast (D_{50} : 42 mm) that ensures effective interlocking of particles thus reducing both l_d and S_v . On the other hand, geogrid $G5$ having larger apertures facilitates the free movement of particles within the aperture of the geogrids. The almost constant values of l_d and S_v for $N > 50,000$ in case of reinforced samples (**Figure 7**) indicate that the effectiveness of ballast-geogrid interlock remains unaffected upon repeated load applications. In a practical sense, this implies that once the required ballast-geogrid interlock is accomplished, the geogrid continues to perform its intended purpose of arresting the lateral displacement and thus reducing the vertical settlement of ballast even at 250,000 load cycles. However, the results indicated that the extent of l_d and S_v increases with the increase in loading frequency but the same are not shown here for the sake of brevity.

Role of Geogrid Aperture Size on the Deformation of Ballast

To highlight the role of geogrid aperture size, the variation of final lateral displacement (l_d) and vertical settlement (S_v) is plotted against A/D_{50} , the ratio of geogrid aperture size to the average particle size of ballast (**Figure 8**). **Figure 8A** shows the variation

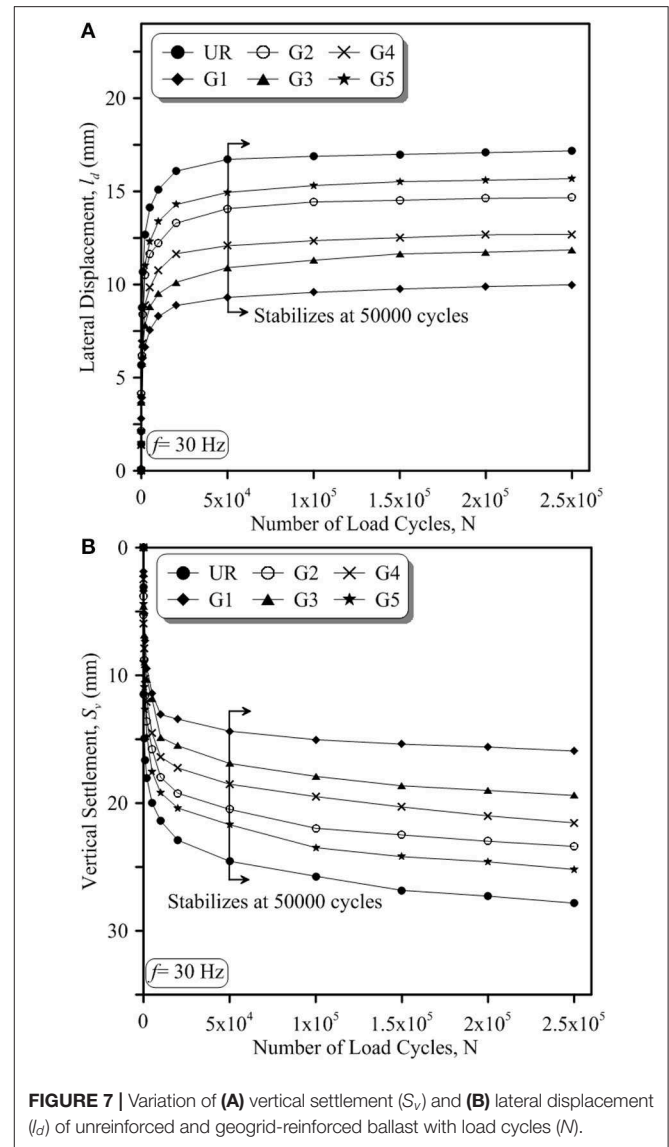


FIGURE 7 | Variation of (A) vertical settlement (S_v) and (B) lateral displacement (l_d) of unreinforced and geogrid-reinforced ballast with load cycles (N).

of l_d of ballast along the depth of ballast layer as measured at levels of five movable plates with A/D_{50} for $f = 30$ Hz. It is revealed that the placement of geogrids at the ballast-sub-ballast interface has shown negligible effect in arresting the lateral displacements at the level of top three plates. However, inclusion of geogrids shows a remarkable effect in reducing the lateral displacements of the bottom two plates. These observations establish beyond doubt the diminishing role of geogrid in arresting particle movements away from its placement position. The role of A/D_{50} is thus evident in the near vicinity of geogrid placement position (i.e., for the bottom two plates). In case of the bottom most plate, the value of l_d decreases from 14.65 to 9.99 mm as A/D_{50} increases from 0.63 to 0.93 which again increases to 15.68 mm at A/D_{50} of 1.54. An increase in lateral displacement at A/D_{50} of 1.54 subsequent to the minimum lateral displacement at A/D_{50} of 0.93 is mainly due to free movement of the particles within the aperture of geogrids.

Figures 8B,C depicts the variation of lateral displacement (l_d) and vertical settlement (S_v) of ballast with A/D_{50} for various

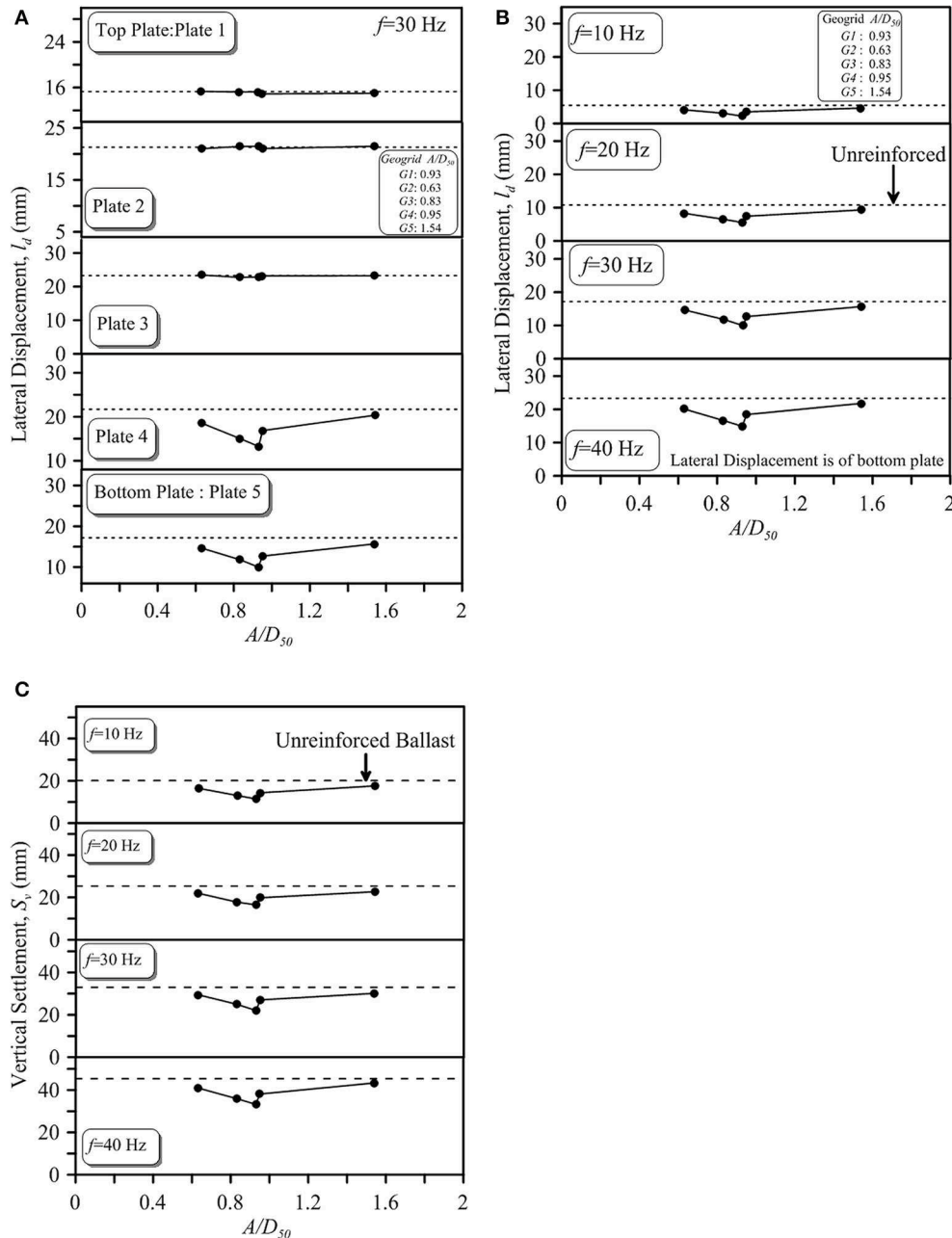


FIGURE 8 | Variation of (A) lateral displacement (l_d) of geogrid-reinforced ballast with A/D_{50} at $f = 30$ Hz, (B) lateral displacement (l_d) with A/D_{50} at different frequencies, and (C) vertical settlement with A/D_{50} at different frequencies.

loading frequencies. It is observed from **Figure 8B** that the value of l_d decreases from 4.14 to 2.25 mm as A/D_{50} increases from 0.63 to 0.93 which then increases to 4.64 mm at A/D_{50} of 1.54 ($f = 10$ Hz). Similarly, the value of S_v decreases from 16.50 to 11.41 mm as A/D_{50} increases from 0.63 to 0.93 and then increases to 17.59 mm at A/D_{50} of 1.54 ($f = 10$ Hz; **Figure 8C**). It is further seen that the variation of l_d and S_v with A/D_{50} remain similar with the increase in loading frequencies albeit with reduced efficiency of geogrids (**Figures 8B,C**). The variation of l_d and S_v with A/D_{50} observed here follows a similar trend as that of variation of

interface efficiency factor with A/D_{50} obtained in case of ballast-sub-ballast interface by Sweta and Hussaini (2019b) under direct shear conditions.

Ballast Breakage Under Cyclic Loading Conditions

To highlight the effect of geogrids in reducing the extent of particle breakage, the initial and final PSDs of unreinforced ballast and that reinforced with geogrids $G1$ and $G5$ at $f = 30$ Hz are compared (**Figure 9A**). The final PSD of the unreinforced

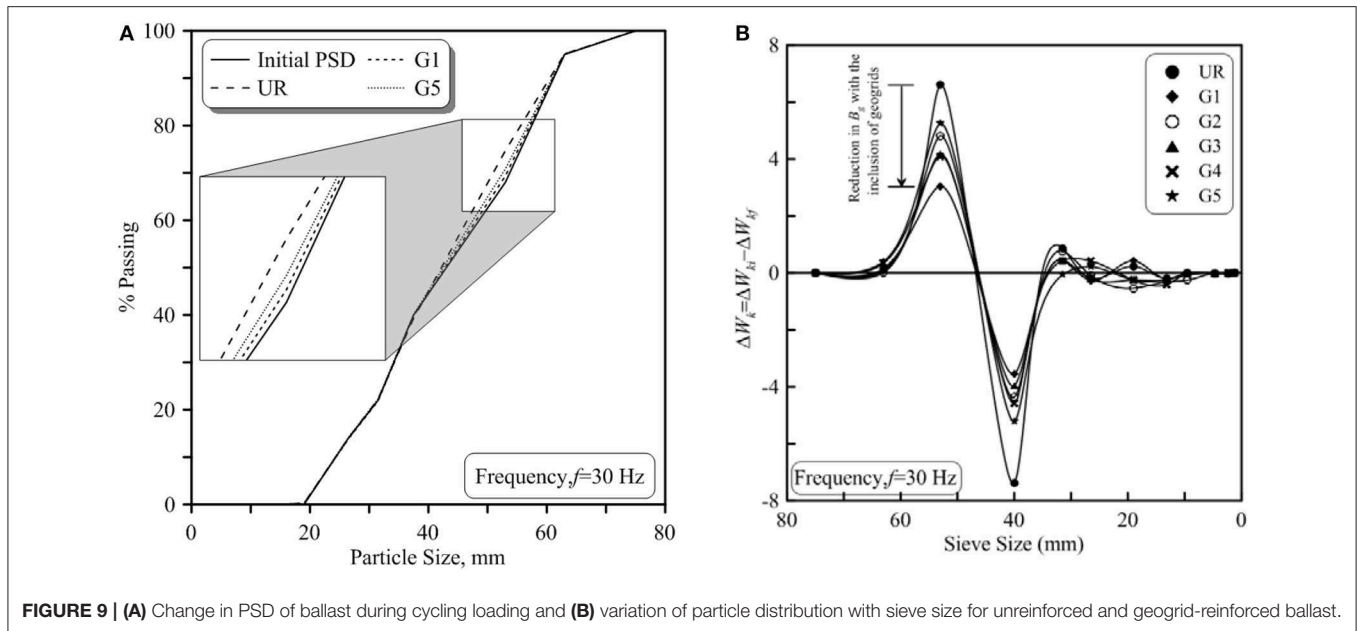


FIGURE 9 | (A) Change in PSD of ballast during cycling loading and **(B)** variation of particle distribution with sieve size for unreinforced and geogrid-reinforced ballast.

ballast lie far away from its initial PSD followed by the final PSD when reinforced with G5 and G1. Although this highlights the role of geogrids in reducing the overall ballast breakage, but its effect on specific particle sizes is seen clearly from **Figure 9B** that shows the variation of difference in percentage retained before and after the test (ΔW_k) at $f = 30$ Hz. It is evident that bigger particles (>40 mm), due to the presence of natural flaws in them and their tendency to take up higher proportions of applied load, are more susceptible to breakage in comparison to the smaller particles. Further, the effect of various geogrids (G1 to G5) in reducing the extent of breakage in bigger particles is also clearly evident from **Figure 9B**, thus justifying their use for stabilizing the rail tracks.

CONCLUSIONS

The current study investigated the shear behavior of geogrid-reinforced ballast-sub-ballast interface and also the deformation and degradation behavior of geogrid-reinforced ballast under cyclic loading conditions. It was revealed that friction (φ) and dilation angles (ψ) of unreinforced ballast-sub-ballast interface reduces from 63.24 to 47.82° and 14.56 to 5.23° with the increase in σ_n and S_r , respectively. The breakage of ballast (B_g) occurred during shearing was quantified in terms of Marsal's Breakage (B_g). The B_g of unreinforced ballast increases from 2.84 to 6.69% with the increase of σ_n & S_r . The tests results further revealed that inclusion of geogrids enhanced the shear strength of ballast-sub-ballast interface. For example, φ of unreinforced ballast-sub-ballast interface increased from 61.82 to 66.02° and ψ decreased from 12.89 to 10.38° when the ballast-sub-ballast interface was reinforced with geogrid G1 ($\sigma_n = 20$ kPa; $S_r = 5.0$ mm/min). Moreover, the extent of B_g in case of direct shear test decreases from 3.33 to 2.49 and 2.56% when stabilized with geogrid G1 and G2, respectively ($\sigma_n = 20$ kPa $S_r = 5.0$ mm/min). The interface

efficiency factor (α) and B_g were found to be function of A/D_{50} ratio. For the set of geogrids tested in the current study, geogrid G1 with an optimum A/D_{50} of 0.93 exhibits the maximum value of α and minimum value of B_g . Moreover, regression model is developed using multiple linear regression analysis to predict the values of φ , ψ , and B_g in terms of the input parameters σ_n , S_r , and A/D_{50} ratio.

The results from the cubical triaxial tests revealed that the deformation and degradation behavior of ballast under cyclic loading conditions was highly influenced by the loading frequency (f). It is shown that the extent of lateral displacement (l_d) and vertical settlement (S_v) increases rapidly during the initial number of load cycles and thereafter it remains constant. The extent of l_d and S_v of unreinforced ballast increases from 5.48 to 28.32 mm and 20.13 to 45.40 mm with the increase in f from 10 to 40 Hz. The value of B_g increased from 4.3 to 11.69% when the value of f was increased from 10 to 40 Hz. It is further revealed that the inclusion of geogrids reduced the extent of l_d and S_v of ballast and minimized the extent the particle breakage during cyclic loading. For instance, insertion of geogrid G1 reduces the extent of l_d and S_v by 42 and 33% , respectively. The current study showed the benefits of geogrids in enhancing the shear strength and also in reducing the deformation and degradation of ballast particles.

DATA AVAILABILITY STATEMENT

All datasets generated for this study are included in the article/supplementary material.

AUTHOR CONTRIBUTIONS

SH and KS have contributed in the preparation of this manuscript.

REFERENCES

- Afzali-Nejad, A., Lashkari, A., and Shourijeh, P. T. (2017). Influence of particle shape on the shear strength and dilation of sand-woven geotextile interfaces. *Geotext. Geomembr.* 45, 54–66. doi: 10.1016/j.geotexmem.2016.07.005
- Anubhav and Basudhar, P. K. (2010). Modeling of soil-woven geotextile interface behavior from direct shear test results. *Geotext. Geomembr.* 28, 403–408. doi: 10.1016/j.geotexmem.2009.12.005
- Anubhav and Basudhar, P. K. (2013). Interface behavior of woven geotextile with rounded and angular particle sand. *J. Mater. Civ. Eng.* 25, 1970–1974. doi: 10.1061/(ASCE)MT.1943-5533.0000774
- Atalar, C., Das, B. M., Shin, E. C., and Kim, D. H. (2001). "Settlement of geogrid-reinforced railroad bed due to cyclic load," in *Proceedings of 15th International Conference on Soil Mechanics and Geotechnical Engineering (Istanbul)*, 2045–2048.
- Bathurst, R. J., and Raymond, G. P. (1987). Geogrid reinforcement of ballasted track. *Transport. Res. Rec.* 1153, 8–14.
- Biabani, M. M., and Indraratna, B. (2015). An evaluation of the interface behavior of rail sub-ballast stabilized with geogrids and geomembranes. *Geotext. Geomembr.* 43, 240–249. doi: 10.1016/j.geotexmem.2015.04.002
- Biabani, M. M., Indraratna, B., and Ngo, N. T. (2016). Modelling of geocell-reinforced sub-ballast subjected to cyclic loading. *Geotext. Geomembr.* 44, 489–503. doi: 10.1016/j.geotexmem.2016.02.001
- Bolton, M. D. (1986). The strength and dilatancy of sands. *Geotechnique* 36, 65–78. doi: 10.1680/geot.1986.36.1.65
- Brown, S. F., Kwan, J., and Thom, N. H. (2007). Identifying the key parameters that influence geogrid reinforcement of railway ballast. *Geotext. Geomembr.* 25, 326–335. doi: 10.1016/j.geotexmem.2007.06.003
- Chen, X., Jia, Y., and Zhang, J. (2018). Stress-strain response and dilation of geogrid reinforced coarse grained soils in large scale direct shear tests. *Geotech. Test. J.* 41, 1–10. doi: 10.1520/GTJ20160089
- Choudhary, A. K., and Krishna, A. M. (2016). Experimental investigation of interface behaviour of different types of granular soil/geosynthetics. *Int. J. Geosynth. Ground Eng.* 2, 1–11. doi: 10.1007/s40891-016-0044-8
- Guler, E., and Khosrowshahi, S. K. (2017). Evaluation of geosynthetic reinforcement on railroad subgrade. *Proc. Eng.* 189, 721–728. doi: 10.1016/j.proeng.2017.05.114
- Hussaini, S. K. K. (2013). *An experimental study on the deformation Behavior of geosynthetically reinforced ballast* (Ph.D. thesis). Wollongong: University of Wollongong, Australia.
- Hussaini, S. K. K., Indraratna, B., and Vinod, J. S. (2012). "Performance of geosynthetically reinforced rail ballast in direct shear conditions," in *11th Australia New Zealand Conference on Geomechanics: Ground Engineering in a Changing World*, eds G.A. Narsilo, A. Arulrajah, and J. Kodikara (Melbourne, VIC: Engineers Australia), 1268–1273.
- Hussaini, S. K. K., Indraratna, B., and Vinod, J. S. (2015a). Application of optical fiber bragg grating sensors in monitoring the rail track deformations. *Geotech. Test J.* 38, 387–396. doi: 10.1520/GTJ20140123
- Hussaini, S. K. K., Indraratna, B., and Vinod, J. S. (2015b). Performance assessment of geogrid reinforced rail road ballast during cyclic loading. *Transport. Geotech.* 2, 99–107. doi: 10.1016/j.trgeo.2014.11.002
- Hussaini, S. K. K., Indraratna, B., and Vinod, J. S. (2016). A laboratory investigation to assess the functioning of railway ballast with and without geogrids. *Transport. Geotech.* 6, 45–54. doi: 10.1016/j.trgeo.2016.02.001
- Indraratna, B., Biabani, M. M., and Nimbalkar, S. (2015). Behavior of geocell-reinforced sub-ballast subjected to cyclic loading in plane-strain condition. *J. Geotech. Geoenviron. Eng.* 141:04014081. doi: 10.1061/(ASCE)GT.1943-5606.0001199
- Indraratna, B., Hussaini, S. K. K., and Vinod, J. S. (2012). On the shear behavior of ballast-geosynthetic interfaces. *Geotech. Test. J.* 35, 305–312. doi: 10.1520/GTJ103317
- Indraratna, B., Hussaini, S. K. K., and Vinod, J. S. (2013). The lateral displacement response of geogrid-reinforced ballast under cyclic loading. *Geotext. Geomembr.* 39, 20–29. doi: 10.1016/j.geotexmem.2013.07.007
- Indraratna, B., Shanin, M. A., and Salim, W. (2007). Stabilisation of granular media and formation soil using geosynthetics with special reference to railway engineering. *Proc. Inst. Civ. Eng. Ground Improv.* 11, 27–43. doi: 10.1680/grim.2007.11.1.27
- Indraratna, B., Thakur, P. K., and Vinod, J. S. (2010). Experimental and numerical study of railway ballast behavior under cyclic loading. *Int. J. Geomech.* 10, 136–144. doi: 10.1061/(ASCE)GM.1943-5622.0000055
- IRSGE (2004). *Specifications for Track Ballast*. Research Design and Standard Organisation (RDSO), Ministry of Railways, India.
- Jeffs, T., and Tew, G. P. (1991). *A Review of Track Design Procedures: Sleepers and Ballast*, Vol. 2. Melbourne, VIC: Railways of Australia.
- Lee, K. M., and Manjunath, V. R. (2000). Soil-geotextile interface friction by direct shear tests. *Can. Geotech. J.* 37, 238–252. doi: 10.1139/t99-124
- Liu, C. N., Ho, Y. H., and Huang, J. W. (2009). Large-scale direct shear tests of soil/PET yarn geogrid interfaces. *Geotext. Geomembr.* 27, 19–30. doi: 10.1016/j.geotexmem.2008.03.002
- Liu, F.-Y., Wang, P., Geng, X., Wang, J., and Lin, X. (2016). Cyclic and post-cyclic behavior from sand-geogrid interface large-scale direct shear tests. *Geosynth. Int.* 23, 129–139. doi: 10.1680/jgein.15.00037
- Liu, H., and Martinez, J. (2015). Creep behavior of sand-geomembrane interfaces. *Geosynth. Int.* 21, 83–88. doi: 10.1680/gein.13.00036
- Liu, S., Huang, H., Qiu, T., and Kwon, J. (2016). Effect of geogrid on railroad ballast particle movement. *Transport. Geotech.* 9, 110–122. doi: 10.1016/j.trgeo.2016.08.003
- Makkar, F. M., Chandrakaran, S., and Sankar, S. (2017). Performance of 3-D geogrid reinforced sand under direct shear mode. *Int. J. Geotech. Eng.* 13, 227–235. doi: 10.1080/19386362.2017.1336297
- Matharu, M. S. (1994). Geogrid cut ballast settlement rate on soft substructures. *Railway Gazette Int.* 150, 165–166.
- Mirzaalimohammadi, A., Ghazavi, M., Roustaei, M., and Lajewardi, S. H. (2019). Pullout response of strengthened geosynthetic interacting with fine sand. *Geotext. Geomembr.* 47, 530–541. doi: 10.1016/j.geotexmem.2019.02.006
- Mishra, D., Qian, Y., Kazmee, H., and Tutumluer, E. (2014). Investigation of geogrid-reinforced railroad ballast behavior using large-scale triaxial testing and discrete element modeling. *Transport. Res. Board.* 2462, 98–108. doi: 10.3141/2462-12
- Moraci, N., Cardile, G., Giofrè, D., Mandaglio, M. C., Calvarano, S. M., and Carbone, L. (2014). Soil geosynthetic interaction: design parameters from experimental and theoretical analysis. *Transport. Infrastr. Geotech.* 1, 165–227. doi: 10.1007/s40515-014-0007-2
- Mvelase, M. G., Grabe, P. J., and Anochie-Boateng, J. K. (2017). The use of laser technology to investigate the effect of railway ballast roundness on shear strength. *Transport. Geotech.* 11, 97–106. doi: 10.1016/j.trgeo.2017.05.003
- Navaratnarajah, S. K., and Indraratna, B. (2017). Use of rubber mats to improve the deformation and degradation behavior of rail ballast under cyclic loading. *J. Geotech. Geoenviron. Eng.* 143:04017015. doi: 10.1061/(ASCE)GT.1943-5606.0001669
- Nimbalkar, S., and Indraratna, B. (2016). Improved performance of ballasted rail track using geosynthetics and rubber shock mats. *J. Geotech. Geoenviron. Eng.* 142:04016031. doi: 10.1061/(ASCE)GT.1943-5606.0001491
- Palmeira, E. M. (2009). Soil-geosynthetic interaction: modeling and analysis. *Geotext. Geomembr.* 27, 368–390. doi: 10.1016/j.geotexmem.2009.03.003
- RDSOGE (2007). *Guidelines for Blanket Layer Provision on Track Formation*. Research Design and Standard Organisation (RDSO), Ministry of Railways, India.
- Sayeed, M. M. A., Ramaiah, B. J., and Rawal, A. (2014). Interface shear characteristics of jute/polypropylene hybrid nonwoven geotextiles and sand using large size direct shear test. *Geotext. Geomembr.* 42, 63–68. doi: 10.1016/j.geotexmem.2013.12.001
- Shin, E. C., Kim, D. H., and Das, B. M. (2002). Geogrid-reinforced railroad bed settlement due to cyclic load. *Geotech. Geol. Eng.* 20, 261–271. doi: 10.1023/A:1016040414725
- Simoni, A., and Houlsby, G. T. (2006). The direct shear strength and dilatancy of sand-gravel mixtures. *Geotech. Geol. Eng.* 24, 523–549. doi: 10.1007/s10706-004-5832-6
- Sun, Q., Indraratna, B., and Ngo, N. T. (2019). Effect of increase in load and frequency on the resilience of railway ballast. *Geotechnique* 69, 833–840. doi: 10.1680/jgeot.17.P.302
- Sun, Q., Indraratna, B., and Nimbalkar, S. (2014). Effect of cyclic loading frequency on the permanent deformation and degradation

- of railway ballast. *Geotechnique* 64, 746–751. doi: 10.1680/geot.14.T.015
- Sweta, K., and Hussaini, S. K. K. (2018). Effect of shearing rate on the behavior of geogrid-reinforced railroad ballast under direct shear conditions. *Geotext. Geomembr.* 46, 251–256. doi: 10.1016/j.geotextmem.2017.12.001
- Sweta, K., and Hussaini, S. K. K. (2019a). Performance of geogrid-reinforced railroad ballast in direct shear mode. *Proc. Inst. Civ. Eng. Ground Improv.* 172, 244–256 doi: 10.1680/jgrim.18.00107
- Sweta, K., and Hussaini, S. K. K. (2019b). Behavior evaluation of geogrid-reinforced ballast-sub-ballast under shear conditions. *Geotext. Geomembr.* 47, 23–31. doi: 10.1016/j.geotextmem.2018.09.002
- Thakur, P. K., Vinod, J. S., and Indraratna, B. (2013). Effect of confining pressure and frequency on the deformation of ballast. *Geotechnique* 63, 786–790. doi: 10.1680/geot.12.T.001
- Vieira, C. S., Lopes, M. L., and Caldeira, L. M. (2015). Sand-geotextile interface characterization through monotonic and cyclic direct shear tests. *Geosynth. Int.* 20, 26–38. doi: 10.1680/gein.12.00037

Conflict of Interest: The authors declare that the research was conducted in the absence of any commercial or financial relationships that could be construed as a potential conflict of interest.

Copyright © 2020 Hussaini and Sweta. This is an open-access article distributed under the terms of the Creative Commons Attribution License (CC BY). The use, distribution or reproduction in other forums is permitted, provided the original author(s) and the copyright owner(s) are credited and that the original publication in this journal is cited, in accordance with accepted academic practice. No use, distribution or reproduction is permitted which does not comply with these terms.

NOMENCLATURE

A	Aperture Size
B_g	Marsal's Breakage Index
C_c	Coefficient of Curvature
C_u	Coefficient of Uniformity
D_{max}	Maximum particle size
D_{50}	Average particle size
f	Loading frequency
l_d	Lateral displacement
ϵ_3	Lateral strain
α	Interface efficiency factor
ϕ	Friction angle
δ	Apparent friction angle for ballast geogrid interface
ψ	Dilation angle
γ_b	Density of ballast
γ_{sb}	Density of sub-ballast
σ_n	Applied normal stress
N	Number of load cycles
PSD	Particle size distribution
S_r	Shearing rate
S_v	Vertical settlement
T_{ult}	Ultimate tensile strength
τ_n	Shear stress
W_k	Percentage weight retained